Avoiding Leakage and Errors Caused by Unwanted Transitions in Lambda Systems

Arian Vezvaee[1,2,*] Evangelia Takou,[1] Paul Hilaire,[1,3] Matthew F. Doty[4] and Sophia E. Economou[1]

[1]*Department of Physics, Virginia Tech, Blacksburg, Virginia 24061, USA*
[2]*Department of Chemistry, University of Colorado at Boulder, Boulder, Colorado 80302, USA*
[3]*Huygens-Kamerlingh Onnes Laboratory, Leiden University, Netherlands*
[4]*Department of Materials Science and Engineering, University of Delaware, Newark, Delaware 19716, USA*

Three-level Λ systems appear in various quantum information processing platforms. In several control schemes, the excited level serves as an auxiliary state for implementing gate operations between the lower qubit states. However, extra excited levels give rise to unwanted transitions that cause leakage and other errors, degrading the gate fidelity. We focus on a coherent-population-trapping scheme for gates and design protocols that reduce the effects of the unwanted off-resonant couplings and improve the gate performance up to several orders of magnitude. For a particular setup of unwanted couplings, we find an exact solution, which leads to error-free gate operations via only a static detuning modification. In the general case, we improve gate operations by adding corrective modulations to the pulses, thereby generalizing the derivative removal by adiabatic gates protocol to Λ systems. Our techniques enable fast and high-fidelity gates and apply to a wide range of optically driven platforms, such as quantum dots, color centers, and trapped ions.

I. INTRODUCTION

Quantum information processing requires the manipulation of quantum bits (qubits) via fast gates with high fidelities. Qubits are formed when a particular two-level subspace is chosen from a larger Hilbert space of a physical system. In specific cases, energy levels outside of the qubit subspace are used as an asset for auxiliary transfer of population within the qubit subspace and for the implementation of quantum gates. An important class of such setups are Λ-type systems that occur in several optically active qubit systems such as self-assembled quantum dots [1–6], nitrogen-vacancy (N-*V*) centers [7–10], trapped ions [11–15], neutral atoms [16], rare-earth ions [17,18], molecular qubits [19], and even in the microwave regime of superconducting circuits [20,21], such as the $0 - \pi$ qubits [22]. Successful manipulation of Λ systems is a key step to perform quantum information processing.

Various methods for the control of Λ systems have been developed [2,3,23–32]. However, in most platforms

———————
*arian.vezvaee@colorado.edu

a bare three-level Λ system is merely an idealization [33]. Unintended interactions with other levels cause leakage and off-resonant couplings that are detrimental to the performance of quantum gates [34,35]. The effect of these off-resonant unwanted couplings is intensified when the extra levels are close in energy to the auxiliary state. In principle, we can use longer pulses to resolve such small splittings. However, the qubit coherence time sets an upper bound to the duration of the pulse. Finding fast pulses that satisfy these opposing constraints and achieve high-fidelity gates is an open problem.

In this paper we develop a novel framework, which enables the design of both fast and high-fidelity qubit gates for Λ systems in the presence of an unwanted transition (Fig. 1); an ubiquitous level structure in many quantum emitter platforms. We derive an analytical solution enabling unit fidelity quantum gates when the two excited states are formed from a set of two basis states. In the general case with no basis states, we develop a new leakage error cancelation strategy based on the derivative removal by adiabatic gates (DRAG) framework to reach high-fidelity gates (with up to 3 orders of magnitude improvements). Former versions of the DRAG method have been widely established as a powerful tool in dealing with unwanted dynamics and leakage cancelations in superconducting qubits [36–40] but, until now, no version of this method was applicable to Λ-type systems [17]
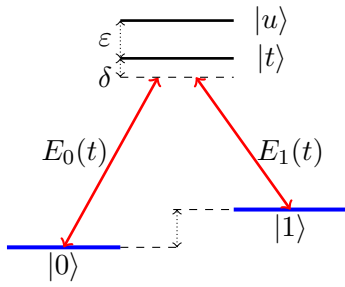
FIG. 1. Schematic depiction of a general Λ-type system with a fourth unwanted level. The qubit is defined in the subspace of the two lower levels $\{|0\rangle, |1\rangle\}$. The coherent control is done through driving the transitions to the target level $|t\rangle$ (with the detuning δ), which is separated from an unwanted level $|u\rangle$ by the splitting ε. The off-resonant coupling to the unwanted level will cause low fidelities. We present resolutions for this problem by introducing a modification to the pulse and the detuning of the system.

due to their indirect control nature via an auxiliary state. Furthermore, our methods come at no additional experimental costs; through gaining physical insight by analyzing the problem in appropriate frames, we infer minimal modifications to the pulse envelope and detuning that correct the errors.

The paper is structured as follows: In Sec. II, we present an overview of the Λ system with an additional ("unwanted") level and the resulting unwanted transitions, and we discuss the relevance of the composition of the target and unwanted levels in terms of a set of two basis states. In Sec. III we start with a hyperbolic secant uncorrected pulse and develop an exact analytical solution in the presence of such a basis-state structure. In Sec. IV we present the case without such a basis-state structure, discuss the DRAG methodology, and develop a new DRAG-based formalism that resolves the off-resonant coupling issue in this case. In Sec. V we analyze the effects of additional errors, namely the crosstalk between the transitions of the Λ system and spontaneous emission. We conclude in Sec. VI. The Appendices contain the technical details of the coherent population trapping (CPT) scheme and our DRAG formalism.

II. Λ SYSTEM WITH UNWANTED TRANSITIONS UNDER CPT

In an ideal three-level Λ system under CPT, the transitions are driven using two external fields [e.g., $E_0(t)$ and $E_1(t)$ in Fig. 1]. Under the two-photon resonance (equal detuning of the two fields from the respective transitions they drive), destructive interference of the transitions caused by the two drive fields leads to the formation of a dark state, i.e., a state that is completely decoupled from the dynamics of the other two levels. This allows us to define the CPT frame, in which the system is described

in terms of two new states in the qubit subspace, the dark state, and its orthogonal bright state (denoted by $|D\rangle$ and $|B\rangle$, respectively), which are superpositions of the $|0\rangle$ and $|1\rangle$ states. Then, the three-level system reduces to a two-level system where transitions are driven between the target excited state and the bright state.

When we implement CPT with pulses that have hyperbolic secant (sech) envelopes, a choice that yields an analytically solvable time-dependent Schrödinger equation in a two-level system [41], we can design arbitrary single-qubit rotations for the Λ system [3]. The parameters of the sech pulses that drive the bright and target state can be chosen such that the evolution is *transitionless* [2]: after the passage of a sech pulse, the population will always return to the bright state, with the bright state acquiring a nontrivial phase

$$\phi = 2\arctan(\sigma/\delta), \tag{1}$$

where σ is the bandwidth, and δ is the detuning. Considering that the bright state spans the full Bloch sphere through the driving field parameters, this leads to full SU(2) qubit control. The technical aspects of the CPT framework and the sech-pulse control are provided in Appendix A. In this work, we are concerned with a nonideal version of this scheme: a Λ system with couplings to an additional, unwanted excited level.

The system under consideration is depicted in Fig. 1; the four states are comprised of a pair of low-energy levels $\{|0\rangle, |1\rangle\}$ that encode the qubit, an auxiliary level $|t\rangle$, which is used to mediate the qubit rotation, and an unwanted level $|u\rangle$. In contrast to the ideal CPT scheme, the additional excited level $|u\rangle$ (separated by an energy splitting ε from the $|t\rangle$ state) introduces competing off-resonant couplings to the qubit states. Our goal is to perform the control of the qubit states using the target level in a way that eliminates or reduces the detrimental effect of the unwanted transition. Throughout this work, for off-resonant drivings, we take the frequency of the control pulses to be smaller than the transition frequency of the target transitions (i.e., negative detuning δ); this choice minimizes the coupling to the unwanted level [42].

Figure 2 shows the fidelity of a $-\pi/2$ rotation about the x axis through direct application of the Λ-system CPT formalism where errors are caused by off-resonant coupling to the unwanted level. In the absence of corrective measures, high fidelity can be obtained only through the use of extremely narrow bandwidth pulses (thus using extremely long pulses in the time domain). In practice however, quantum gates should be implemented within the coherence time of the system and before it relaxes to its ground states through spontaneous emission. The relaxation time of relevant solid-state quantum emitters is usually short (e.g., approximately 1 ns in quantum dots [43], 1.85 ns in silicon vacancy [44], 4.5 ns in tin vacancy [45], and
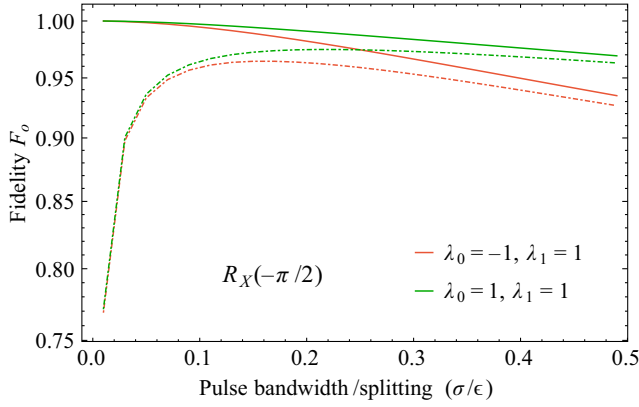
FIG. 2. Fidelity of an X rotation by $-\pi/2$, $R_X(-\pi/2)$, in terms of the dimensionless parameter pulse bandwidth over splitting (σ/ε). Here, σ is the bandwidth of the sech pulse and ε is the splitting between the unwanted and target levels. The fidelities are shown for two cases of dependent [$\lambda_0 = -\tan(\pi/4) = -1/\lambda_1$] and independent ($\lambda_0 = 1, \lambda_1 = 1$) couplings. Without any corrective measures and ignoring spontaneous emission, reasonable fidelities required for quantum information processing are only achievable by using extremely narrow bandwidth pulses (solid lines). However, upon inclusion of spontaneous emission (dashed lines), even narrow bandwidth pulses will not lead to perfect fidelities.

10 ns in N-V centers [46]), thus requiring broad bandwidth pulses in general. We develop a formalism that deals with the issue of off-resonant couplings without trading off the duration of the gates for selectivity, ensuring operations performed within the relaxation time. The effects of spontaneous emission are further discussed in Sec. V A.

As mentioned above, the two transitions of the Λ system are distinct and each transition is driven by a single drive field [$E_0(t)$ or $E_1(t)$], as shown in Fig. 1. This can be satisfied by either polarization selection rules or large energy separation of the ground states, depending on the specifics of the platform considered. In the former case, the orthogonality of each transition dipole with one drive field ensures that each transition couples to a single drive. In the latter case, sufficient energy separation of the ground-state levels implies that the off-resonant couplings of the drive fields to the opposite Λ transitions average out. We relax this assumption and discuss the effects of the crosstalk in Sec. V B. In the following, we first discuss different scenarios for the composition of the target and unwanted levels that lead to different dynamics of the system. We discuss physical examples corresponding to each scenario in Sec. VI

In a generic setup where no particular composition for the target and unwanted levels is assumed, the dipole moments between the qubit states and the target level are defined as $d_{0,t} \equiv \langle t|d|0\rangle$ and $d_{1,t} \equiv \langle t|d|1\rangle$. Similarly, for the dipole moments between the qubit states and the unwanted level we have $d_{0,u} \equiv \langle u|d|0\rangle$ and $d_{1,u} \equiv \langle u|d|1\rangle$.

The coupling to the unwanted level can then be quantified by the ratio of the transition dipole moments $\lambda_0 \equiv d_{0,u}/d_{0,t}$ and $\lambda_1 \equiv d_{1,u}/d_{1,t}$. By setting the target level dipole moments to unity we have the Rabi frequencies $\Omega_0(t)$ and $\Omega_1(t)$ for the target transitions, and $\lambda_0\Omega_0(t)$ and $\lambda_1\Omega_1(t)$ for the unwanted transitions, respectively. We label the effective couplings λ_0 and λ_1 arising from the scenario as *independent couplings*, since they are independent from each other.

Alternatively, there may be scenarios in which the target and unwanted levels originate from a set of two basis states $|b_0\rangle$ and $|b_1\rangle$, with, e.g., a field mixing the two. This leads to couplings that depend on one another (see Sec. VI for physical examples). In this scenario $|t\rangle = \sin(\eta)|b_1\rangle - \cos(\eta)|b_0\rangle$ and $|u\rangle = \cos(\eta)|b_1\rangle + \sin(\eta)|b_0\rangle$, where $|0\rangle$ couples only to $|b_0\rangle$, and $|1\rangle$ couples only to $|b_1\rangle$, with dipole moments d_{0,b_0} and d_{1,b_1}, respectively. In this case, a coupling parameter η determines the weight of the composition of the two basis states. Moreover, since $|0\rangle$ couples only to $|b_0\rangle$, we have the Rabi frequency $\Omega_0(t) \equiv -\cos(\eta)d_{0,b_0}E_0$. Similarly, since $|1\rangle$ couples only to $|b_1\rangle$ the Rabi frequency $\Omega_1(t) \equiv \sin(\eta)d_{1,b_1}E_1$. This choice translates into a set of couplings to the unwanted level given by λ_0 (for the $|0\rangle \leftrightarrow |u\rangle$ transition driven by E_0) and λ_1 (for the $|1\rangle \leftrightarrow |u\rangle$ transition driven by E_1), that are inversely proportional: $\lambda_0 \equiv -\tan(\eta) = -1/\lambda_1$. Therefore, we label the couplings arising from this scenario as *dependent couplings*, since there is a relation between them through the coupling parameter η.

In the following we discuss the errors caused by each of the cases above and develop methods that allow implementation of fast and high-fidelity gates. We leave the numerical simulations regarding the nature of the errors in each case (that is, phase error versus leakage), until Sec. VI where we develop enough methodology. In Sec. III, we discuss that the errors from the case of dependent couplings [$\lambda_0 \equiv -\tan(\eta) = -1/\lambda_1$] are mostly phase errors and we can achieve quantum gates with negligible error simply by modifying the drive frequency. We discuss the case of independent couplings in which the errors are due to leakage in Sec. IV where we develop a novel version of the DRAG method to achieve high-fidelity gates in these systems.

III. DEPENDENT COUPLINGS: AN EXACT SOLUTION APPROACH

In this section, we first consider the Λ system with an additional excited state formed from basis states that lead to dependent couplings. The additional excited state induces off-resonant couplings outside of the Λ subspace, which in the CPT frame translates into transitions that link the bright and dark states to the unwanted level. In an ideal Λ system, one would drive the target transitions with the

fields $E_\ell(t) = \Omega_{\ell,o}(t)\cos(\omega_\ell t)$ ($\ell = 0, 1$), and static detuning δ to implement the desired gate operation. Here o refers to the original drive fields, described by the unperturbed hyperbolic secant envelopes, and ω_ℓ is the drive frequency. The resonant frequencies for the transitions $|0\rangle \leftrightarrow |t\rangle$ and $|1\rangle \leftrightarrow |t\rangle$ are denoted as ω_{0t} and ω_{1t}, respectively; the detuning δ is defined as $\delta = \omega_0 - \omega_{0t} = \omega_1 - \omega_{1t}$. In the following, as is standard for CPT, we make use of the rotating wave approximation (RWA), i.e., we define $E_\ell(t) = \exp(-i\omega_\ell t)\Omega_{\ell,o}(t) + \text{c.c.}$.

Although our formalism is general and applicable to the design of arbitrary axis single-qubit gates, we choose to showcase our protocols in the particular context of X gates (or equivalently Y gates, up to a phase between the two drives). For this reason, we set the two Rabi frequencies of the target transitions (i.e., $|0\rangle \leftrightarrow |t\rangle$ and $|1\rangle \leftrightarrow |t\rangle$) to be equal, that is $\Omega_o \equiv \Omega_{0,o} = \Omega_{1,o}$. Under this condition and RWA, the Hamiltonian in the CPT frame rotating with the drive frequency is given by (see Appendix A for derivation):

$$H_{\text{CPT}} = (\delta/2)(\Pi_D + \Pi_B - \Pi_t - \Pi_u) + \varepsilon\Pi_u$$
$$+ \left\{ \sqrt{2}\Omega_o |B\rangle\langle t| + \frac{1}{\sqrt{2}}\Omega_o(\lambda_0 - \lambda_1)|D\rangle\langle u| \right.$$
$$\left. + \frac{1}{\sqrt{2}}\Omega_o(\lambda_0 + \lambda_1)|B\rangle\langle u| + \text{h.c.} \right\}, \quad (2)$$

where $\Pi_m = |m\rangle\langle m|$. Notice that the CPT Hamiltonian above is generic since the relation among the λ_0 and λ_1 are kept implicit. However, in this section we consider the case of dependent couplings: $\lambda_0 \equiv -\tan(\eta) = -1/\lambda_1$. As discussed in Sec. II, in the dependent couplings case the parameter η can be tuned, and interestingly enough, it can be tuned such that it allows for a decoupling condition that transforms the four-level system into two two-level systems. That is, when $\eta = \pi/4$ (equivalently $\lambda_0 = -1$, $\lambda_1 = 1$), the four-level system in the CPT frame transforms into two independent two-level systems, each driven by a sech pulse (Fig. 3): the bright and target, and the dark and unwanted. For a single two-level system, the population returns to the ground state at the end of the evolution if the absolute value of the Rabi frequency is equal to the bandwidth of the pulse (see Appendix A). For $\eta = \pi/4$ this condition is satisfied for both two-level systems. Under this condition, we can therefore solve analytically the problem as it separates into two separate two-level problems. This enables us to find an exact solution, where the unwanted level is fully taken into account and its dynamics are incorporated into the gate design. We note that the two two-level structure that we uncovered above, which can be thought of as a double-CPT phenomenon, only becomes evident upon the analysis of the system in the CPT frame. As we show in Appendix A, the typical analysis of the system in the lab frame masks this interesting property of the problem.
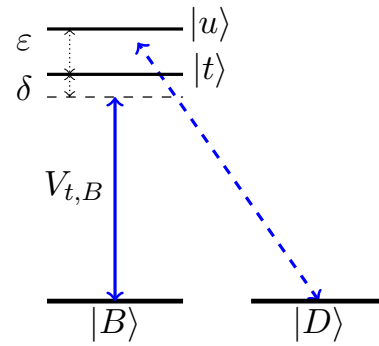
FIG. 3. Selection rules in the dressed basis of CPT in the case of equal couplings, i.e., $\eta = \pi/4$. In this case the problem reduces to two dissociated two levels (bright and target, and dark and unwanted), each subject to a transitionless pulse.

The difference in the dynamics of the two two-level systems arises from the different detunings; each ground state acquires a different phase at the end of the evolution. Thus, the total phase (rotation angle in the bright-dark subspace) will be $\phi_{\text{tot}} = \phi_{B,t} - \phi_{D,u}$, where $\phi_{B,t} = 2\arctan(\sigma/\delta)$, and $\phi_{D,u} = 2\arctan(\sigma/(\delta - \varepsilon))$. Therefore, the error in implementation of the desired gate is caused by the deviation of ϕ_{tot} from the intended phase in the bright-dark subspace. We can account for this phase difference by writing ϕ_{tot} as

$$\phi_{\text{tot}} = 2\arctan\left(\frac{-\sigma\varepsilon}{(\delta - \varepsilon)\delta + \sigma^2}\right), \quad (3)$$

and then obtain the detuning modification required for the exact implementation of any desired rotation angle. To implement a rotation by $\phi_{\text{tot}} = -|\phi|$, we find

$$\delta = \frac{1}{2}\left(\varepsilon \pm \sqrt{\varepsilon^2 + 4\varepsilon\sigma\cot\left[\frac{|\phi|}{2}\right] - 4\sigma^2}\right). \quad (4)$$

By setting the detuning to either branch of the equation above, a $-|\phi|$ rotation with negligible gate error will be implemented. For instance, $R_X(-\pi/2)$ and $R_X(-\pi)$ are illustrated in Fig. 4. These gate performances are quantified by averaging over all input states existing in the Hilbert space, which can be reduced to the following expression [47]:

$$F_i = \frac{1}{6}\sum_{j=\pm x,\pm y,\pm z}\text{Tr}\left[U_{\text{ideal}}\rho_j U_{\text{ideal}}^\dagger \mathcal{U}_i(\rho_j)\right]. \quad (5)$$

Here, the ρ_j's are the six cardinal states on the Bloch sphere, $\mathcal{U}_i(\rho_j)$ is the evolution of the axial vectors under the actual evolution of the system, and i is either the original or the exact solution. The ideal evolution in the subspace of $\{|D\rangle, |B\rangle\}$ is given by $U_{\text{ideal}} = \text{diag}(e^{-i\phi}, e^{i\phi})$, where ϕ is given by Eq. (1). We use this quantification of the gate performances throughout the rest of this paper.
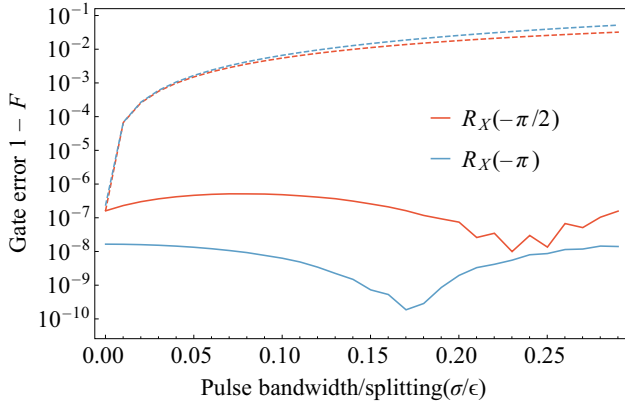
FIG. 4. $R_X(-\pi/2)$ and $R_X(-\pi)$ rotations for pulses with no correction (dashed) and exact modifications of detuning (solid) given by Eq. (4), in terms of the dimensionless parameter bandwidth over splitting (σ/ε). The gate times of the sech pulses are chosen to be $16/\sigma$ and the nonmonotonic behavior of $R_X(-\pi)$ is due to negligible numerical instability rising from cutting off the sech pulses. This exact approach for $\eta = \pi/4$ enables gate implementation with negligible gate error.

It is noteworthy that, as Fig. 4 shows, without pulse shaping and chirping, or increased experimental overhead, we can realize unit fidelity operations by incorporating the unwanted level into our quantum control design. Notice that an idealized sech pulse would be infinitely long. In our numerical simulations, however, we need to set a finite gate time on the pulse. By increasing the length of the pulse, the resulting errors in Fig. 4 will become smaller, and, in the limit of infinitely long pulses, the error completely vanishes.

As we move further away from this particular setup of dependent coupling strengths $\eta = \pi/4$, the two two-level systems become coupled. Nevertheless, our analytic solution still gives rise to substantial gate improvement. We define the gate improvement as the ratio of the original gate error to the gate error using the improved solution. This is shown in Fig. 5. As seen from the figure, away from $\eta = \pi/4$ the gate performance improves, with of course the best improvement occurring near $\eta \approx \pi/4$ where the two two-level system formation of CPT frame is valid.

To summarize this section, we have shown that for equal two-photon detunings, equal Rabi frequencies (for X rotations), and $\eta = \pi/4$, the system transforms into two two-level systems, for which the dynamics can be solved exactly according to Eq. (4). Moreover, this decoupling into two two-level systems can occur for any arbitrary rotations, upon correct choice of Rabi frequencies in the CPT frame. However, the two two-level systems' formation does not necessarily occur in the case of independent couplings. More generally, if the two couplings have the same sign, then the errors will not be in the form of phase errors anymore. For this reason, when the couplings are independent we resort to a different strategy based on perturbative expansion methods, as we describe in the following section.

IV. INDEPENDENT COUPLINGS: DRAG FORMALISM WITH CPT

In this section, we consider the case of a Λ system with an additional unwanted level, where the couplings to the auxiliary states are independent of each other but have the same sign. To gain insight into how the CPT-transformed
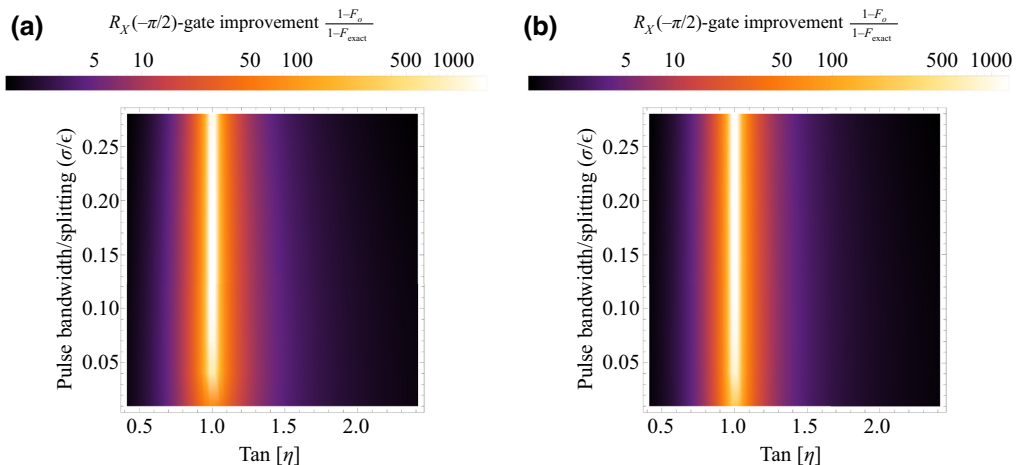
FIG. 5. Gate improvement of (a) $R_X(-\pi)$ and (b) $R_X(-\pi/2)$, in terms of the dimensionless parameter pulse bandwidth over splitting (σ/ε), and the parameter η, which determines the weight distributions of the basis states in the target and unwanted levels $|t\rangle = \sin(\eta)|b_1\rangle - \cos(\eta)|b_0\rangle$ and $|u\rangle = \cos(\eta)|b_1\rangle + \sin(\eta)|b_0\rangle$. The best improvements occur for when the two dissociated two-level approximation is valid ($\eta \approx \pi/4$). However, even away from this value, the exact solution leads to substantial gate improvements, through a single modification of the detuning.

Hamiltonian [Eq. (2)] in the system would look in a limiting case, we may consider when the couplings are equal to each other and have the same strength as the coupling to the target level: $\lambda_0 = \lambda_1 = 1$. It can be seen from Eq. (2) that in this case the system turns into a V-type system rather than two dissociated two-level systems. The errors, in this case, will not be a simple phase error that can be taken care of by modification of the detuning. In fact, as we demonstrate in Sec. VI, the source of errors, in this case, is leakage to the unwanted level. Therefore, we develop a novel version of the DRAG method tailored to CPT that allows the implementation of high-fidelity gate operations. The details of our DRAG methodology are presented in Appendix B.

To overcome the errors for the present case via the DRAG approach, we start by modulating the original pulses. We consider an additional correction $\Omega_{\ell,c}(t)$ ($\ell = 0, 1$) to each of the two fields, phase detuned from the original drive by $\pi/2$. We further set the frequency to be the same as that of the original drive, hence reducing the experimental overhead of an additional laser drive. From here on, we use the letter c to refer to any subsequent parameters of the corrective drive fields. We choose the total fields of the system to be $E_\ell(t) = (1/2)\Omega_{\ell,o}(t)\cos(\omega_\ell t) + (1/2)\Omega_{\ell,c}(t)\sin(\omega_\ell t)$, which in RWA are equivalent to $E_\ell(t) = (1/2)\exp(-i\omega_\ell t)(\Omega_{\ell,o}(t) + i\Omega_{\ell,c}(t)) + $ c.c. Following the previous section, we apply our formalism to the context of X rotations, so we set the two Rabi frequencies of the target transitions to be equal, with an additional condition on the corrective fields:

$$\Omega_o \equiv \Omega_{0,o} = \Omega_{1,o},$$
$$\Omega_c \equiv \Omega_{0,c} = \Omega_{1,c}. \tag{6}$$

We note that these conditions can be lifted and the formalism we develop remains valid, with the difference that the rotation axis changes.

Under these conditions and after performing the RWA, the Hamiltonian in the CPT frame is given by (see Appendix A)

$$\tilde{H}_{\text{CPT}} = (\delta/2)(\Pi_B + \Pi_D - \Pi_t - \Pi_u) + \varepsilon\Pi_u$$
$$+ \frac{1}{2\sqrt{2}}\Big\{ 2\sum_{j=o,c}\Omega_j\sigma_{B,t}^j + (\lambda_0 - \lambda_1)\sum_{j=o,c}\Omega_j\sigma_{D,u}^j$$
$$+ (\lambda_0 + \lambda_1)\sum_{j=o,c}\Omega_j\sigma_{B,u}^j\Big\}, \tag{7}$$

where to indicate the matrix elements for the generic transition $|m\rangle \leftrightarrow |n\rangle$, we define $\sigma_{m,n}^o \equiv |n\rangle\langle m| + |m\rangle\langle n|$ and $\sigma_{m,n}^c \equiv i|n\rangle\langle m| - i|m\rangle\langle n|$. Previous formulations of the DRAG method have focused on canceling out leakage errors in ladder-type systems (e.g., transmons) that occur

between consecutive energy levels, making it inapplicable to Λ systems since the qubit control is performed indirectly via the target level. We develop the appropriate version of DRAG for this problem in the following.

Under the DRAG formalism, corrections to the driving fields are determined by utilizing a frame transformation $A(t) = e^{-iS(t)}$ [39]:

$$H_{\text{DRAG}} = A^\dagger(t)\tilde{H}_{\text{CPT}(t)}A(t) + i\dot{A}^\dagger(t)A(t). \tag{8}$$

The operator $S(t)$ can be any arbitrary Hermitian operator as long as it respects the boundary conditions of the transformation. That is, the frame transformation has to vanish at the beginning and end of the pulse ($A(0) = A(t_g) = \mathbf{1}$), such that the ideal gate we wish to design remains the same in both the CPT and DRAG frames. Given the generality of $S(t)$, extracting closed-form pulse solutions is nontrivial for our four-level system (since the pulses are time dependent), hence, we turn to a perturbative expansion of the transformation. To that end, we utilize the Schrieffer-Wolff (SW) transformation [48] and its perturbative expansion. Additionally, we expand the CPT Hamiltonian of Eq. (7) into a power series of $x = 1/\varepsilon t_g$ (see Appendix B for details).

Our goal is to constrain the DRAG-frame Hamiltonian such that it implements the intended ideal evolution. To this end, we define a target Hamiltonian, capable of performing arbitrary rotations within the qubit (dark-bright) subspace,

$$H_{\text{target}}^{\text{CPT}}(t) = \frac{1}{2}\sum_{i=o,c}h_i(t)\sigma_{B,t}^i + \frac{1}{2}h_z(t)\left(\Pi_B - \Pi_t\right), \tag{9}$$

where $h_i(t)$ and $h_z(t)$ are arbitrary control fields. Here we choose the $h_i(t)$ to be sech pulses. To ensure that the DRAG frame Hamiltonian implements the intended operation as dictated by $H_{\text{target}}^{\text{CPT}}$, we impose the following constraints:

$$\text{Tr}[H_{\text{DRAG}}(t)\sigma_{B,t}^i] = h_i(t),$$
$$\text{Tr}[H_{\text{DRAG}}(t)\left(\Pi_B - \Pi_t\right)] = h_z(t), \tag{10}$$

where $i \in \{o, c\}$. Additionally, to enforce decoupling from the unwanted subspace in the new Hamiltonian, we impose the following constraints:

$$\text{Tr}[H_{\text{DRAG}}(t)\sigma_{D,u}^i] = 0,$$
$$\text{Tr}[H_{\text{DRAG}}(t)\sigma_{B,u}^i] = 0, \tag{11}$$
$$\text{Tr}[H_{\text{DRAG}}(t)\sigma_{t,u}^i] = 0,$$

where $i \in \{o, c\}$. The constraints can be solved consistently and lead to a set of corrective pulses for each order of the expansion. The details of the derivation for the corrective fields can be found in Appendix B. For the X rotation with

conditions (6), the simplest solutions lead to the following modifications to each pulse:

$$\Omega_{0,o}(t) = \Omega_{1,o}(t) = \sqrt{2}\left(1 + \delta\frac{(\lambda_0 + \lambda_1)^2}{16\varepsilon}\right)\Omega(t), \quad (12)$$

$$\Omega_{0,c}(t) = \Omega_{1,c}(t) = \frac{\sqrt{2}}{16\varepsilon}(\lambda_0 + \lambda_1)^2\dot{\Omega}(t). \quad (13)$$

Notice that, each transition is still subject to a single pulse since we combine the modified original envelope and the phase-shifted correction into a single new pulse $\Omega_i(t) = \Omega_{i,o}(t) + i\Omega_{i,c}(t)$. We depict the sech pulse envelopes and their derivatives for one specific set of parameters in Fig. 6.

Due to the indirect control of the qubit via auxiliary states in Λ systems, the diagonal constraint of Eq. (10),

does not lead to a global phase among all states for the first-order DRAG Hamiltonian. Instead, it resolves the off-resonant coupling at the cost of inducing a phase between the bright and dark states. Therefore, we need to investigate the form of the first-order DRAG Hamiltonian to infer this phase between the dark and bright states. By restricting our attention to the Λ system subspace, we find the zeroth-, and first-order DRAG frame Hamiltonian in the subspace of $\{|D\rangle, |B\rangle, |t\rangle\}$ to be

$$H_{\mathrm{DRAG}}^{(0)} = \begin{bmatrix} \delta/2 & 0 & 0 \\ 0 & \delta/2 & \Omega(t) \\ 0 & \Omega(t) & -\delta/2 \end{bmatrix}, \quad (14)$$

and

$$H_{\mathrm{DRAG}}^{(1)} = \begin{bmatrix} -\frac{1}{8\varepsilon}(\lambda_0 - \lambda_1)^2\,\Omega^2(t) & \frac{1}{8\varepsilon}\left(-\lambda_0^2 + \lambda_1^2\right)\Omega^2(t) & 0 \\ \frac{1}{8\varepsilon}\left(-\lambda_0^2 + \lambda_1^2\right)\Omega^2(t) & -\frac{1}{16\varepsilon}(\lambda_0 + \lambda_1)^2\,\Omega^2(t) & 0 \\ 0 & 0 & -\frac{1}{16\varepsilon}(\lambda_0 + \lambda_1)^2\,\Omega^2(t) \end{bmatrix}. \quad (15)$$

Notice that for the limiting case of a V-system (i.e., $\lambda_0 = \lambda_1 = 1$), all elements of $H_{\mathrm{DRAG}}^{(1)}$ in Eq. (15) vanish, except for the diagonal entry of the bright state. While the zeroth-order DRAG Hamiltonian stays in the form enforced by Eqs. (10), we note that in the first-order DRAG Hamiltonian there is an induced phase between the dark state and the bright-target subspace. In this Hamiltonian [Eq. (15)], the bright and target states follow the same

phase evolution, as dictated by the common diagonal element $-1/(16\varepsilon)(\lambda_0 + \lambda_1)^2\Omega^2(t)$. However, the qubit states are composed of the dark and bright states, which up to the first order (neglecting the off-diagonal elements of $H_{\mathrm{DRAG}}^{(1)}$) evolve with a different phase. Effectively, this implies that the DRAG corrections reduce the unintended off-resonant couplings to the unwanted level at the cost of inducing a relative phase between the qubit states in the CPT frame. This is an immediate consequence of the fact that we counteract the unwanted couplings indirectly; in the CPT frame, we design a target Hamiltonian that involves transitions between the bright and target levels. The discussion above sheds light on an important physical insight into designing any DRAG-based method for qubits with indirect control via an auxiliary state. In the following we discuss the approximation above, highlighting how significantly indirect control of the qubit affects designing our DRAG-based approach.

We note that the unwanted subspace in Eq. (15) is neglected, since these elements constitute a higher-order error. This arises from the fact that in Eq. (8), the nth order DRAG Hamiltonian includes contributions from $S^{(n+1)}(t)$. The off-diagonal entries in the qubit subspace in Eq. (15) are difficult to incorporate analytically, unlike the transmon case [38] where the off-diagonal entries are identically zero and the diagonal phase evolution is the same for both qubit states. In contrast, the selection rules of the Λ systems require incorporating the fact that the DRAG corrections will induce a phase difference on dark and bright
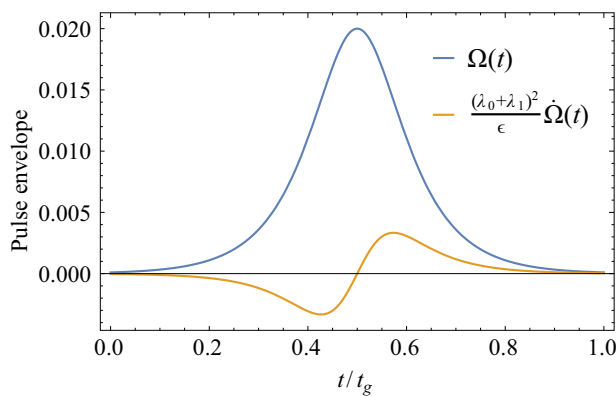
FIG. 6. An example of pulse shapes for a system with splitting of $\varepsilon = 80\,\mu\mathrm{eV}$. The sech pulse (in blue) is $\Omega(t) = \sigma\,\mathrm{sech}(\sigma(t - t_g/2))$, and its derivative corrective solution (in orange) modulated with the splitting and the couplings is $\Omega(t) = (\lambda_0 + \lambda_1)^2(1/\varepsilon)(d/dt)\sigma\,\mathrm{sech}(\sigma(t - t_g/2))$. The bandwidth is taken to be $\sigma = 0.02\,\mathrm{meV}$, and gate time is $t_g = 16/\sigma$.
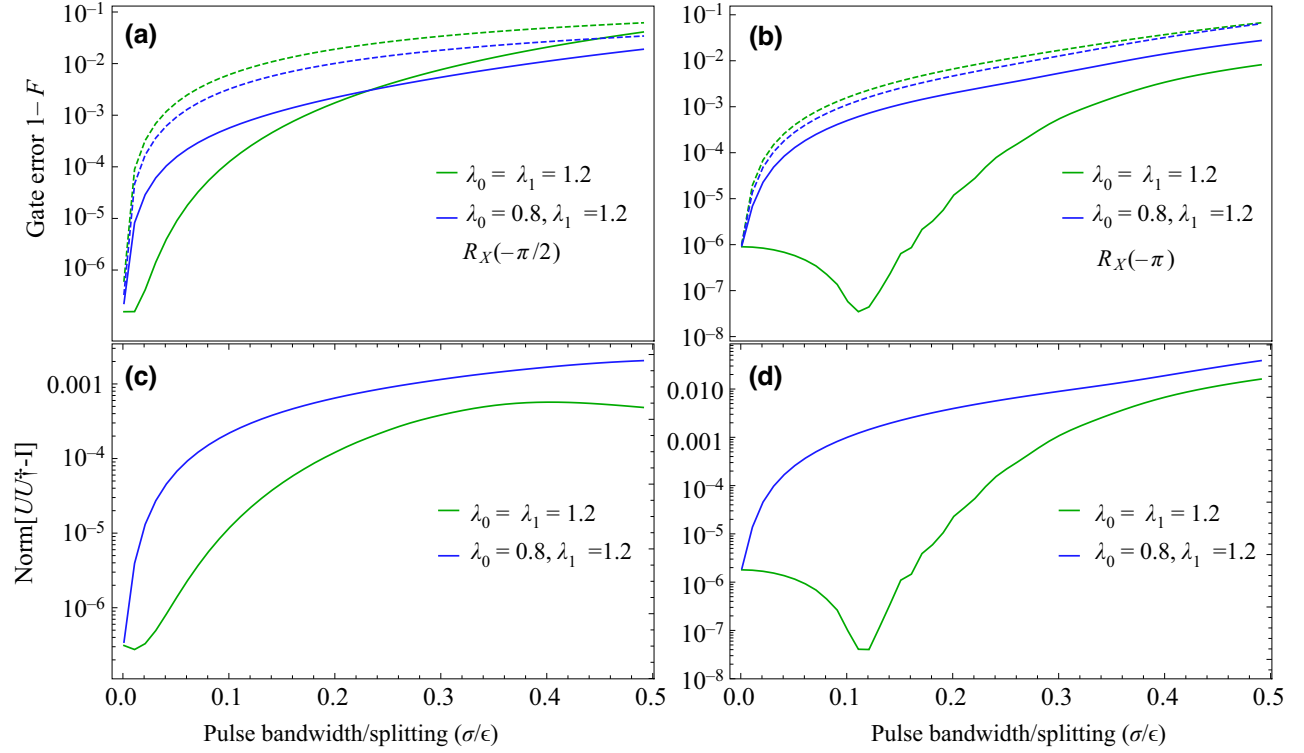
FIG. 7.   Gate-error comparison in terms of the dimensionless parameter pulse bandwidth over splitting (σ/ε) for the original pulse (dashed) and DRAG solution (solid) for (a) $-\pi/2$ and (b) $-\pi$ rotation about the x axis. (c),(d) Corresponding deviation from unitarity ($|UU^\dagger - \mathbf{1}|$) of (a),(b), respectively. The colors correspond to different strengths of couplings to the unwanted level.

states (diagonal entries), whereas the off-diagonal terms constitute a higher-order error.

We now highlight the procedure for finding the required detuning modification, on top of the pulse modulation, to correct for the phase error caused by the implementation of DRAG. We showcase this for the case of $\lambda_0 = \lambda_1 = 1$ because, as we discuss above, it only leads to an induced phase between the bright and dark states up to the first order. To this end, we denote the ideal evolution operator that corresponds to $H_{\mathrm{DRAG}}^{(0)}$ as U_0; this is the analytically solvable time-evolution operator (which is also the ideal gate in the CPT frame). Our total Hamiltonian, $H_{\mathrm{DRAG}} = H_{\mathrm{DRAG}}^{(0)} + H_{\mathrm{DRAG}}^{(1)}$, evolves with a time evolution given by $U(t) = U_0(t)U(t)'$, and satisfies the equation:

$$i\dot{U}_0 U' + iU_0\dot{U}' = (H_{\mathrm{DRAG}}^{(0)} + H_{\mathrm{DRAG}}^{(1)})U_0 U', \quad (16)$$

which reduces to

$$i\dot{U}' = (U_0^\dagger H_{\mathrm{DRAG}}^{(1)} U_0)U', \quad (17)$$

where U' is the evolution operator of $H_{\mathrm{DRAG}}^{(1)}$ in the interaction picture of $H_{\mathrm{DRAG}}^{(0)}$. Given the fact that the first-order error in $H_{\mathrm{DRAG}}^{(1)}$ are the diagonal entries, we focus only on the bright-target subspace. In this subspace, $H_{\mathrm{DRAG}}^{(1)} \propto$

$g(t)\mathbf{1}$, where $g(t)$ is the function that defines the relative phase shift between the dark and bright states. Solving the Schrödinger equation we find that the induced phase is given by $\theta = -(\lambda_0^2 + \lambda_1^2 - 6\lambda_0\lambda_1)\sigma/(4\varepsilon)$. Hence, in order to remove the θ shift from the target evolution we modify the detuning:

$$\delta \rightarrow \delta' = \sigma/\tan\left(\frac{\phi + \theta}{2}\right), \quad (18)$$

where ϕ is the target rotation angle. The detuning modification (18) together with Eqs. (12) and (13) complete our full set of solutions for the pulses. The final pulse shapes will depend on the specific details of the system such as the splitting of the two auxiliary states.

We demonstrate the performance of the DRAG solutions in Fig. 7. The figure shows the fidelity of rotations about the x axis, i.e., $R_X(-\pi)$ and $R_X(-\pi/2)$ gates, in terms of the dimensionless parameter given by the pulse bandwidth over the splitting between the target and unwanted levels. We consider the case in which both transitions are of equal strength larger than that with respect to the target level ($\lambda_0 = \lambda_1 = 1.2$) and the case of unequally strong couplings with one larger and one smaller than the coupling to the target state ($\lambda_0 = 0.8, \lambda_1 = 1.2$). The top panels of Fig. 7 show the gate error of implemented operations and
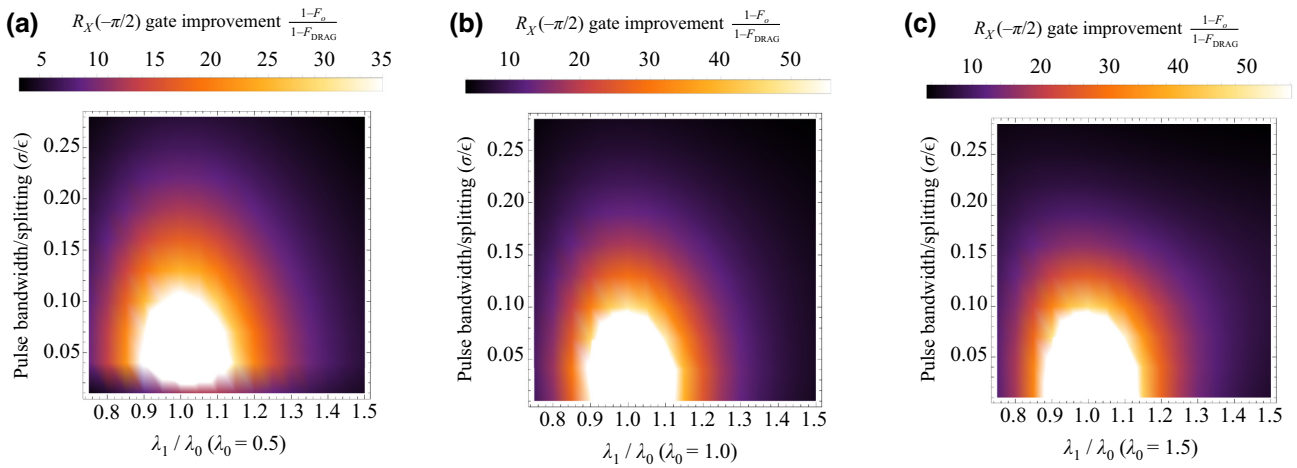
FIG. 8. $R_X(-\pi/2)$-gate improvements for three different cases of coupling strengths to the unwanted level [for (a) $\lambda_0 = 0.5$, (b) $\lambda_0 = 1$, (c) $\lambda_0 = 1.5$], as a function of the bandwidth over splitting, with respect to the ratio of the unwanted couplings. Local maxima in gate improvements corresponds to the presence of local minima in the gate error (see Fig. 7); at these certain values, the unitarity condition is satisfied, therefore, the DRAG formalism becomes more effective.

the bottom panels shows the deviation from unitarity of the operators, defined as $|UU^{\dagger} - \mathbf{1}|$. It is clear from these plots that our DRAG correction provides substantial improvement compared to the uncorrected gate, in some cases by several orders of magnitude. It can also be seen that the operators do not remain unitary for the whole range of bandwidths over splittings, which indicates that the populations are leaving the qubit subspace. This signals that the sources of errors in this case are leakage, rather than phase errors, unlike the case of dependent couplings in Sec. III. As such, our devised DRAG solution performs better at ranges of bandwidths over splittings where the gate implementation remains unitary, but it always provides an improvement throughout the full bandwidth range.

In Fig. 8, we show the improvement in the fidelity of the $R_X(-\pi/2)$ gate as a function of both the bandwidth over splitting and the ratio of the unwanted couplings for three different values of these couplings with respect to the coupling to the target state (which is set to unity in all cases). In all cases, the best DRAG improvements occur at points where the values of the couplings are similar to each other, i.e., $\lambda_0 = \lambda_1$. The local maximum gate improvements near these values are due to the occurrence of gate-error minima that are related to the corresponding deviation from unitarity values: at these specific parameter values of the system, the transitionless condition is being satisfied and therefore the DRAG decoupling from the unwanted state becomes more efficient. Furthermore, notice that because our pulse corrections are functions of the couplings, improvements are more effective for the cases where the unwanted couplings are stronger compared to the coupling to the target state (i.e., λ_0, $\lambda_1 > 1$). In these cases, since the original fidelities are lower due to strong couplings, DRAG improves the gate error by several orders of magnitude,

as opposed to the weak couplings where DRAG could only make slight improvements since the original fidelity is relatively high regardless.

While the $\lambda_0 \sim \lambda_1$ case (equivalently $\eta \approx \pi/4$ in the exact scenario of Sec. III) leads to the best improvements, let us formalize the discussion above by describing how our protocol covers *all* the possible scenarios in which the two unwanted couplings differ significantly from one another. Three scenarios are possible to occur: (I) $\lambda_0 \gg \lambda_1$, while $\lambda_0, \lambda_1 > 1$. This would indicate that an improper choice of target versus coupling transitions was made; one can swap the target and unwanted levels and the presented analysis in our formalism will be indeed the same. (II)
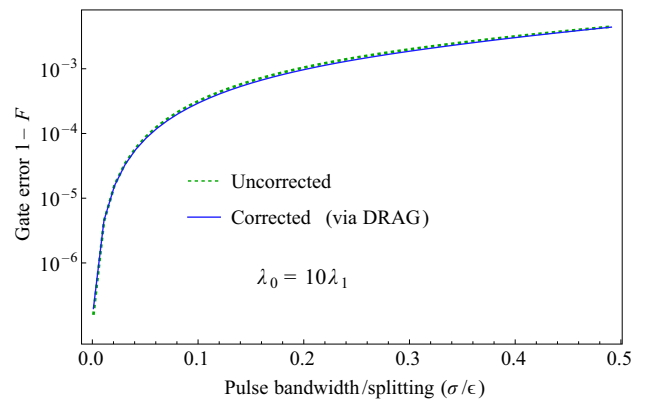
FIG. 9. The gate errors for $R_X(-\pi/2)$ gate versus pulse bandwidth over splitting in the scenario when $\lambda_0 \gg \lambda_1$. The dashed curve corresponds to the uncorrected case, and the solid curve to the case when we modulate the pulse envelopes based on the DRAG solutions. As the figure demonstrates, in this case the weak coupling is a practically negligible transition and as such, the gate errors are already in the order of 10^{-4}–10^{-3}.
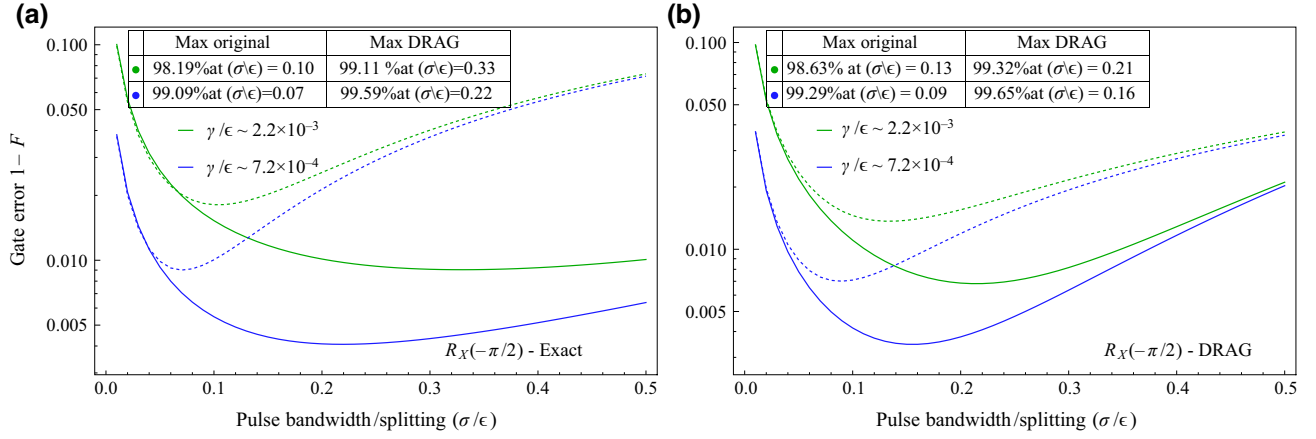
FIG. 10.   The effects of spontaneous emission on $R_X(-\pi/2)$ using (a) exact with $\tan(\eta) = 1.2$ and (b) DRAG solutions with $\lambda_0 = 1.2, \lambda_1 = 0.8$, for two different values of spontaneous emission in terms of the dimensionless ratio of the decay rate and the splittings γ/ε: 2.2×10^{-3} and 7.2×10^{-4}. In each case the dashed lines are original pulses and the solid lines are the improved pulses. The inset values indicate the maximum fidelities and the corresponding bandwidths. With no corrective measures, best fidelities occur at narrow bandwidths. Our modified pulses lead to better fidelities at higher pulse bandwidths.

$\lambda_0 \gg \lambda_1$, while $\lambda_0, \lambda_1 < 1$: in this case the *improvement* is not significant since the the uncorrected gate errors are in the order of 10^{-4}–10^{-3} (see Fig. 9). (III) $\lambda_0 \sim \lambda_1$, while $\lambda_0, \lambda_1 < 1$: this is in fact the scenario that is encountered most often and across a variety of platforms. Control in this regime is challenging because the system does not exhibit dominant transitions and all coupling strengths are comparable. We discuss a variety of physical platforms relevant to this regime in Sec. VI.

V. EFFECTS OF ADDITIONAL ERRORS

In this section, we consider the effects of errors other than the off-resonant couplings to the unwanted level to examine how the performance of our solutions is affected. In particular, we focus on two important sources of error: spontaneous emission from the excited levels and crosstalk between the transitions of the Λ system.
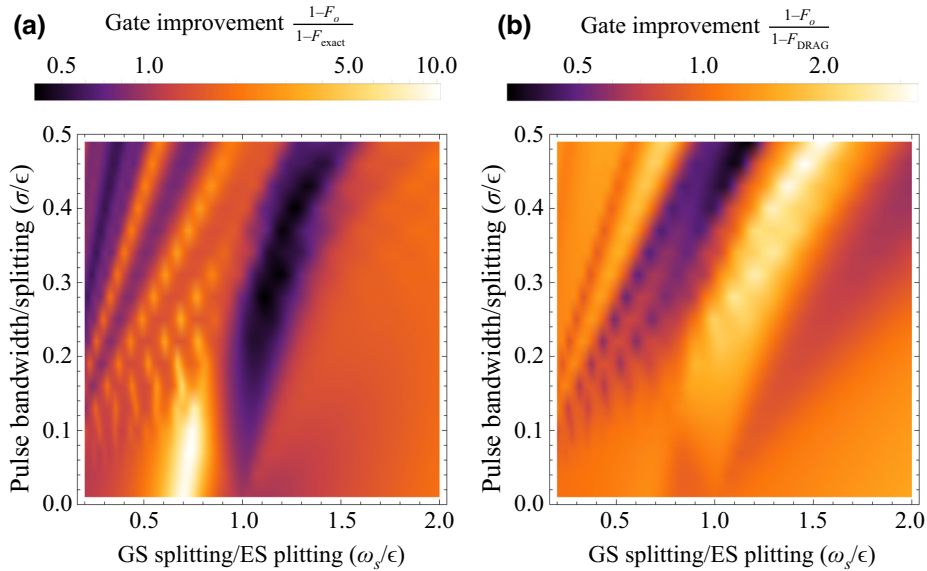
FIG. 11.   Gate improvement of $R_X(-\pi/2)$ for (a) the exact method and (b) using the DRAG method, including the crosstalks between the two transitions of the Λ system. The vertical axis is the dimensionless parameter pulse bandwidth over the excited states' splitting (σ/ε), and the horizontal axis is the dimensionless parameter ground states' splitting over the excited states' splitting (ω_s/ε). The other parameter values are $\eta = \pi/4$ for the exact method, and $\lambda_0 = 1, \lambda_1 = 1$ ($\kappa_{01} = 1 = 1/\kappa_{10}$).

A. Spontaneous emission

A realistic optically active system is coupled to the environment and therefore relaxes through the spontaneous emission of photons. This relaxation process reduces the fidelity of our intended quantum gates, more severely impacting longer gates. We describe the dynamics with a standard open quantum system approach to model the effects of spontaneous emission. We use the Liouville-von Neumann equation with Lindblad relaxation terms: $\dot{\rho} = -i[H, \rho] + \mathcal{L}[\rho]$, where $\mathcal{L}[\rho] = \sum_{ij} \left(L_{ij} \rho L_{ij}^\dagger - \frac{1}{2} \left[L_{ij}^\dagger L_{ij} \rho + \rho L_{ij}^\dagger L_{ij} \right] \right)$. The Lindblad operators account for the populations that leave the target and unwanted levels upon emission of a photon. We pick four Lindblad operators that correspond to emission from each excited state to each ground state: $L_{ij} = \sqrt{\gamma} |i\rangle \langle j|$, where $i \in \{0, 1\}$, $j \in \{t, u\}$, and γ is the emission rate, which we take to be the same for all transitions.

We consider the effects of spontaneous emission for both cases of dependent and independent couplings. Figure 10 shows the effects of spontaneous emission on the corrected exact and DRAG solutions for different dimensionless values of γ/ε, for $R_X(-\pi/2)$. As evident from the figure, we see that two opposing effects are acting on the system. On one hand, the detrimental effect of the unwanted

level favors short-bandwidth pulses. On the other hand, the spontaneous emission favors large-bandwidth pulses (i.e., short pulses in time). This results in a minimum gate error for an intermediate value of the pulse bandwidth. (In the DRAG case, notice that this is independent of deviation from unitarity condition discussed in the previous section.) The insets in Fig. 10 show the maximum obtainable value of fidelities with their corresponding values of bandwidth over splitting. For both values of γ/ε, while the corrective solutions lead to a better maximum fidelity, they also occur at larger values of bandwidth over splitting. Therefore our formalism provides us with better gate performances, at more reasonable values of pulse bandwidths, suitable for systems with fast spontaneous emission rates.

B. Crosstalk

So far in our discussion we assume that either the polarization selection rules or the energy separation of the ground states allow the two transitions of the Λ system to be distinguished. Here we include the error from crosstalk of the two transitions. We model our interaction picture crosstalk Hamiltonian (for an X rotation) in the frame rotating with the frequency of the pulses, as follows:

$$
\begin{aligned}
H_{\mathrm{CT}} = {} & (\delta/2)(\Pi_0 + \Pi_1 - \Pi_t - \Pi_u) + \varepsilon \Pi_u + \big\{ (1/2)(\Omega_o - i\Omega_c)(1 + e^{-i\omega_s t}\kappa_{10})|0\rangle\langle t| \\
& + (1/2)(\Omega_o - i\Omega_c)(\lambda_0 + e^{-i\omega_s t}\lambda_0 \kappa_{10})|0\rangle\langle u| + (1/2)(\Omega_o - i\Omega_c)(1 + e^{-i\omega_s t}\kappa_{01})|1\rangle\langle t| \\
& + (1/2)(\Omega_o - i\Omega_c)(\lambda_1 + e^{-i\omega_s t}\lambda_1 \kappa_{01})|1\rangle\langle u| + \text{h.c.} \big\}.
\end{aligned}
\tag{19}
$$

Here ω_s quantifies the ground-state (GS) splitting (i.e., the splitting between the qubit states, $|0\rangle$ and $|1\rangle$, in the lab frame). Following the assumption on the transition dipoles discussed in Sec. II, the crosstalk couplings may also be implicitly dependent or independent of each other. When the E_0 (E_1) field drives the $|1\rangle \to |t\rangle$ ($|0\rangle \to |t\rangle$) transition, it leads to crosstalk coupling $\kappa_{01} = E_0/E_1$ ($\kappa_{10} = E_1/E_0$). Consequently, once the E_0 field drives the $|1\rangle \to |u\rangle$ transition, the resulting crosstalk coupling will be $\lambda_1 \kappa_{01}$, and similarly, the effect of E_1 driving the $|0\rangle \to |u\rangle$ transition will be the coupling $\lambda_0 \kappa_{10}$.

Figure 11 shows the effect of crosstalk on the gate improvement of $R_X(-\pi/2)$ for both the exact and the

DRAG method. The values are shown for a range of dimensionless parameters of pulse bandwidths over excited-state (ES) splittings (σ/ε), and GS splitting over ES splitting (ω_s/ε). In (a), for the exact method, we set $\eta = \pi/4$ and in (b), for the DRAG method, we set $\lambda_0 = 1, \lambda_1 = 1$. Furthermore, the ratio of the two electric fields is chosen to be unity $E_1/E_0 = 1$ (i.e., $\kappa_{01} = 1 = 1/\kappa_{10}$). As the figure indicates, the behavior of the improvement heavily relies on the specific parameters of the system. For example, the crosstalk Hamiltonian corresponding to Fig. 11(a) (i.e., $\lambda_0 = -1, \lambda_1 = 1$) in the CPT frame after RWA will be,

$$
\begin{aligned}
\tilde{H}_{\mathrm{CT,CPT}} = {} & (\delta/2)(\Pi_B + \Pi_D - \Pi_t - \Pi_u) + \varepsilon \Pi_u + \frac{1}{\sqrt{2}} \Big\{ i(1 + \cos(\omega_s t)) \sum_{j=o,c} \Omega_j \sigma_{B,t}^j \\
& + (-i)\sin(\omega_s t) \sum_{j=o,c} \Omega_j \sigma_{D,t}^j + (-i)\sin(\omega_s t) \sum_{j=o,c} \Omega_j \sigma_{B,u}^j + i(1 + \cos(\omega_s t)) \sum_{j=o,c} \Omega_j \sigma_{D,u}^j \Big\}.
\end{aligned}
\tag{20}
$$

(a) Gate improvement $\frac{1-F_o}{1-F_{exact}}$

(b) Gate improvement $\frac{1-F_o}{1-F_{DRAG}}$
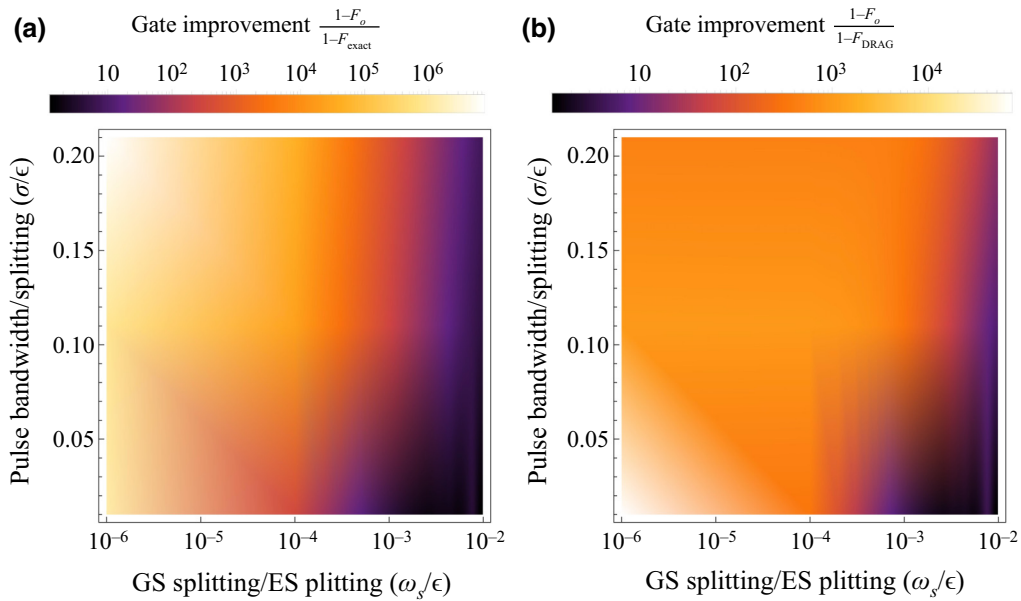
FIG. 12. $R_X(-\pi/2)$ gate improvement with crosstalks in the regime that $\varepsilon \gg \omega_s$ for (a) the exact method and (b) the DRAG method. In addition to the corrective measures, the Rabi frequencies are also multiplied by $1/2$ due to the crosstalk modifications to the system Hamiltonian (see the text). The other parameter values are $\eta = \pi/4$ for the exact method, and $\lambda_0 = 1, \lambda_1 = 1$ ($\kappa_{01} = 1 = 1/\kappa_{10}$).

This indicates that, firstly, the pulse profiles will be modulated with some time-dependent, periodic functions of ω_s, therefore the pulse behavior will be nontrivial. Additionally we notice that for $\varepsilon \gg \omega_s$, the system reduces to that of two two-level systems. This means that in this regime our exact solution is applicable. Similarly, looking at the corresponding Hamiltonian to Fig. 11(b) (i.e., $\lambda_0 = 1, \lambda_1 = 1$) we find that in the same $\varepsilon \gg \omega_s$ limit, it reduces to that of the V system for which we develop the DRAG formalism. Both of these cases require a slight correction of Rabi frequencies by a factor of $1/2$ to account for additional factor of 2 arising from this terms $1 + \cos(\omega_s t)$. We show the performance of these solutions in the presence of crosstalk in Fig. 12. As seen in both figures, improvements of several orders of magnitude are achievable through our approaches given that the condition $\varepsilon \gg \omega_s$ is satisfied. We also note that in the case of dependent couplings, because the errors are in the form of phase errors, in principle, it is possible to track the phase change and correct it through detuning modification. Moreover, for a generic DRAG-based approach to avoid the crosstalks in Λ systems we refer to the work in Ref. [49].

VI. DISCUSSION AND CONCLUSION

In summary we have developed a framework to achieve fast high-fidelity control in Λ systems with unwanted transitions; a setup that is ubiquitous to many different platforms. More importantly, our methods come at a minimal experimental cost, only requiring slight modifications to the pulse envelope or the detuning of the driving, informed

by physical insight from careful analysis of the problem at hand. In particular, we have shown that for the two cases, depending on the existence of a basis structure in the target and unwanted levels (which determines whether the corresponding couplings are dependent or independent of one another) the approach to correcting for the unwanted level is distinct.

The case of the dependent couplings arises due to the mixing of two basis states in the excited-state manifold. This occurs, for example, in the form of symmetric and antisymmetric superposition states in $0 - \pi$ superconducting qubits. The protection of $0 - \pi$ qubits against relaxation and pure dephasing leads to the appearance of these symmetric and antisymmetric states that will cause unwanted transitions in the Λ systems [22]. Similarly, in quantum dot molecules where the qubit states are the spinor projection of a single hole, both the $|t\rangle$ and $|u\rangle$ states are created by the bonding and anti-bonding superpositions of two different charge and spin configurations, with the coupling mediated by tunneling. In this example, the degree of mixing can be controlled through applied electric fields [34,50]. This scenario is also expected in single self-assembled quantum dots in a transverse magnetic field, which changes the selection rules to the so-called Voigt geometry.

We showed that in this dependent-couplings case the Λ system reduces to a combination of two two-level systems in the limit of equal basis weights ($\eta = \pi/4$). We further discussed that the errors are in the form of phase errors; as such we devised an exact solution that compensates for these errors in the form of detuning modifications and
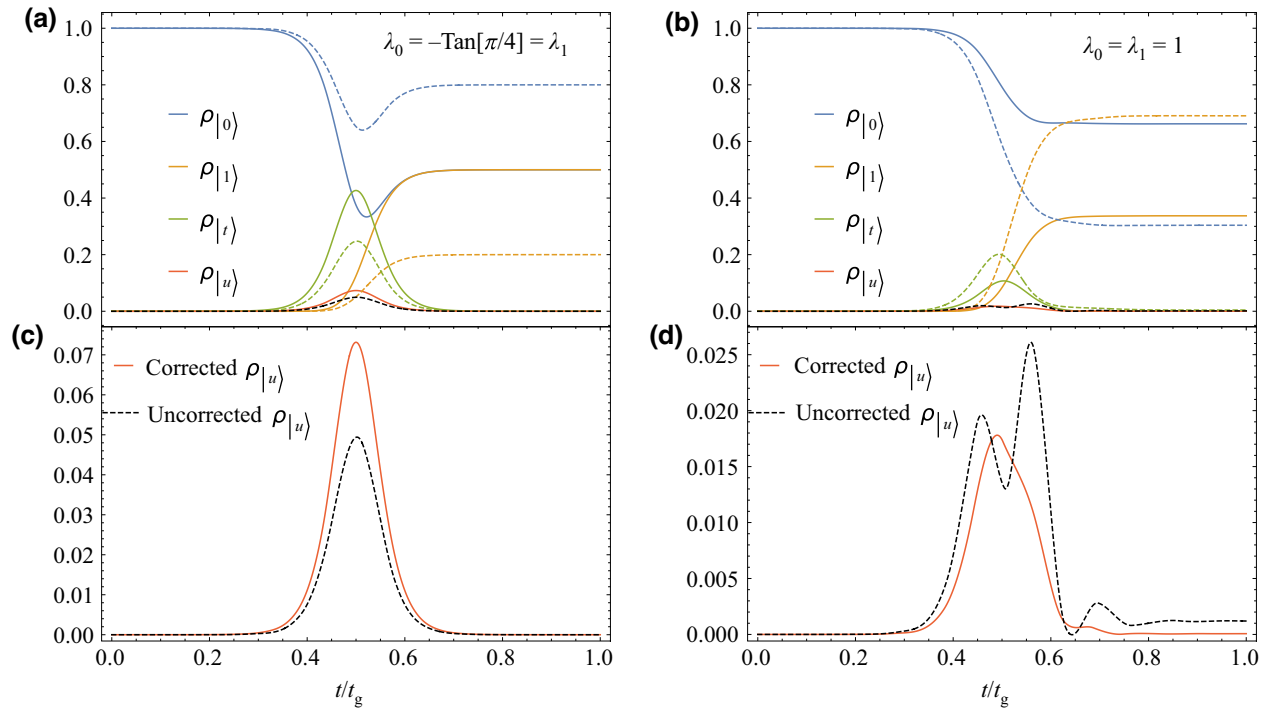
FIG. 13. The dynamics of population during $R_X(-\pi/2)$ gate for all four levels of a Λ system with an unwanted level. In (a) we use the exact method (for dependent couplings), and in (b) we have used the DRAG method (for independent couplings of same sign). The bandwidth over splitting ratio is taken to be $\sigma/\varepsilon = 0.5$. The dashed curves indicate the populations of a nonmodified system and the solid lines indicate populations of a system subject to our modified solutions. Bottom panels (c),(d), are specifically focused on the population of the unwanted level for (a),(b), respectively. The populations of target and unwanted levels subject to a transitionless pulse go back to the qubit states at the end of the gate time in (a),(c). However, in the case of dependent couplings in (b),(d), we deal with leakage to unwanted level. Both of our designed formalisms correct the population of the qubit levels with respect to desired gate, and additionally, our DRAG method reduces the leakage in (d).

allows for error-free gate implementations. On the other hand, in the absence of basis states, the system turns into a V system in the limiting case of equal couplings with the same sign. In this system the source of errors has the form of leakage rather than phase errors. In Sec. IV we developed a new version of the DRAG approach to battle the leakage in this case. An example of this scenario occurs in color centers, such as the group-IV defects in diamond. In particular, in the absence of external magnetic fields, one could select laser fields with different polarizations to form a Λ system, which leads to independent couplings [49].

To see the different form of errors of each coupling scenario (i.e., phase error versus leakage), we briefly comment on the evolution of population of each level during the gate time. In Fig. 13 we have shown the populations of the system for a $R_X(-\pi/2)$ rotation, for the cases of both dependent and independent couplings. The transitionless nature of the pulses driving two independent two-level systems is evident in Fig. 13(c): the final population of excited states are negligible for both uncorrected and corrected solutions. This indicates that the core of the errors in our system are the phase errors due to the off-resonant couplings to unwanted states, rather than leakage. Our

formalism corrects these errors by populating the excited states appropriately and redistributing the populations on the qubit states such that the desired gates are implemented. On the other hand, as we discussed in Sec. IV, in the independent couplings case the evolution of the system is nonunitary. As such, by the end of the gate time some of the population leaves the qubit subspace, being stored in the unwanted level [Fig. 13(d)]. Our DRAG approach battles this leakage through modulation of the pulses and restores the full population to the qubit subspace. However, this comes at the price of inducing some phase errors, which are compensated through the additional detuning modification.

In summary, the two methods we present above are capable of implementing high-fidelity arbitrary gates in either case of a Λ system with unwanted transitions. The exact method has the advantage that it requires only a simple modification of the detuning. The DRAG pulse modification, on the other hand, is in the form of a corrective modification to the original pulse shape that drives each transition of the system.

It should be noted that the DRAG pulse modulation solution is not unique; we have made specific choices

on the generative parameters of the DRAG frame in deriving our DRAG solutions (see Appendix B for details of the derivations). These generative elements are the free parameters of the system and can be set to arbitrary values as long as they satisfy the DRAG transformation condition $S(t_g) = S(0) = 0$. Therefore, alternative DRAG solutions based on different generative elements can also be devised. We have demonstrated such pulse shapes in Fig. 6. The corrective pulse is inversely proportional to the splitting ε and the coupling to the unwanted level for that transition [Eq. (13)]. For smaller splittings, the correction pulse becomes more comparable to the original pulse. Furthermore, as we mentioned below Eqs. (12) and (13), we emphasize that even though the mathematical derivation of the pulse design is phrased in terms of an original (uncorrected) pulse and a correction, experimentally the full corrected pulse would be programmed and generated directly.

Finally, we discussed the implementation of X, and Y rotations. To achieve universal control of the qubit system, we also require implementations of Z rotations. This can be done either through the same control scheme by driving only a single transition of the Λ system with a sech pulse [2] or simply through "virtual" Z gates [51]. The exact solution and the version of DRAG we have tailored to the case of a Λ system with a fourth unwanted level are general and can be applied to a variety of optically active qubits, such as color centers (e.g., the N-V center in diamond), trapped ions, rare-earth ions, self-assembled quantum dots, and quantum dot molecules.

ACKNOWLEDGMENTS

APPENDIX A: COHERENT POPULATION TRAPPING

In this Appendix, we present the mathematical details of the CPT framework. Two-level systems subject to a sech pulse with Rabi frequency Ω and bandwidth σ, can be solved analytically [41] and the solutions are in the form of hypergeometric functions. For the case of $\Omega/\sigma \in \mathbb{N}$, these pulses are transitionless [2], i.e., after the passage of the pulse the population will always return to the ground state with the ground state acquiring a nontrivial phase ϕ [Eq. (1)] through the process. For the specific case of $\Omega = \sigma$, the Hamiltonian of a generic two-level system driven by a sech pulse in the rotating frame is given by

$$H = \begin{pmatrix} 0 & \Omega(t)e^{-i\delta t} \\ \Omega(t)e^{i\delta t} & 0 \end{pmatrix}, \qquad (A1)$$

where $\Omega(t) = \sigma \operatorname{sech}(\sigma(t - t_g/2))$. For this system the unitary evolution operator at the end of the gate is $U = \operatorname{diag}(e^{-i\phi}, e^{i\phi})$. As shown in Ref. [3], in the CPT scheme, the transitions of the system are excited using the drive field, $E_0 f_0(t)e^{i\omega_0 t} + e^{i\alpha}E_1 f_1(t)e^{i\omega_1 t} +$ h.c. For identical temporal envelopes and detunings, with Rabi frequencies $\Omega_0(t)$ and $\Omega_1(t)$, the transformation of the original qubit states to the bright and dark states is given by

$$\begin{pmatrix} |D\rangle \\ |B\rangle \end{pmatrix} = \begin{pmatrix} \cos\frac{\theta}{2} & -e^{i\alpha}\sin\frac{\theta}{2} \\ e^{-i\alpha}\sin\frac{\theta}{2} & \cos\frac{\theta}{2} \end{pmatrix} \begin{pmatrix} |0\rangle \\ |1\rangle \end{pmatrix}, \qquad (A2)$$

where $\sin(\theta/2) = \Omega_0/\Omega_{\text{eff}}$, $\cos(\theta/2) = \Omega_1/\Omega_{\text{eff}}$, and $\Omega_{\text{eff}}^2 = \Omega_0^2 + \Omega_1^2$. In the CPT frame, the transition matrix elements between the target and the dark state vanishes and the bright and target state will have the matrix element defined by the effective Rabi frequency: $V_{t,B} = \Omega_{\text{eff}} f(t) e^{-i\delta t}$. For the case of both drives using a sech temporal envelope, i.e., $f_0(t) = f_1(t) = \operatorname{sech}(\sigma t)$, the transitionless pulse with $\Omega_{\text{eff}} = \sigma$ will induce the relative phase ϕ between the bright and dark states, which translates to a rotation in the subspace of $|D\rangle$ and $|B\rangle$. Therefore, by varying the drive parameters we can set the unitary transformation of Eq. (A2) to transform our original qubit states to the desired states in the CPT frame, effectively enabling the rotation about an arbitrary axis of rotation $\hat{n} = (\sin\theta\cos\alpha, \sin\theta\sin\alpha, \cos\theta)$: $R_n(\phi) = e^{-i\phi\hat{n}\cdot\vec{\sigma}}$. We refer the readers to Ref. [3] for further details of the CPT scheme subject to sech pulses.

The CPT framework can be applied to the case of the Λ system with an unwanted level in a similar way. However, there will be additional transitions from the bright and dark state to the unwanted level. In the lab frame of a nonideal system with an unwanted level, for the case of equal detunings δ, the Hamiltonian in the interaction frame after the RWA can be written as

$$H_{\text{int}} = \sum_{j=0,1} e^{i(\delta-\varepsilon)t}\lambda_j\Omega_j|j\rangle\langle u| + \sum_{j=0,1} e^{i\delta t}\Omega_j|j\rangle\langle t| + \text{h.c.} \qquad (A3)$$

The CPT transformation for an X rotation amounts to having both Rabi frequencies to be equal: $\Omega_o(t) = \Omega_0(t) = \Omega_1(t)$ (we set $\theta = \pi/2$ and $\alpha = 0$). Such CPT transformation turns this Hamiltonian into

$$H_{\text{CPT}} = e^{i\delta t}\sqrt{2}\Omega_o|B\rangle\langle t| + \frac{e^{i(\delta-\varepsilon)t}}{\sqrt{2}}\Big\{\Omega_o(\lambda_0 - \lambda_1)|D\rangle\langle u| + \Omega_o(\lambda_0 + \lambda_1)|B\rangle\langle u|\Big\} + \text{h.c.} \qquad (A4)$$

We proceed by removing the oscillatory parts of the CPT Hamiltonian by going to a rotating frame. We do this using

the frame transformation

$$\text{diag}\left[e^{-i(\delta/2)t}, e^{-i(\delta/2)t}, e^{i(\delta/2)t}, e^{i(\delta/2-\varepsilon)t}\right]. \quad (A5)$$

Upon this transformation we arrive at the Hamiltonian given by Eq. (2) of the main text. Repeating the same series of transformations outlined above, but now this time with the additional controls $\Omega_{\ell,c}(\ell = 0, 1)$ under the condition $\Omega_o \equiv \Omega_{0,o} = \Omega_{1,o}$, and $\Omega_c \equiv \Omega_{0,c} = \Omega_{1,c}$, leads to the Hamiltonian given in Eq. (7).

APPENDIX B: MATHEMATICAL DERIVATION OF DRAG SOLUTIONS

In this Appendix, we lay out the details of our DRAG-based formalism that leads to the solutions presented in Eqs. (12) and (13). To that end, we employ the perturbative DRAG theory developed in Ref. [38] as the base of our formalism. First, we make the CPT Hamiltonian dimensionless by multiplying all quantities by the gate time t_g and expand the Hamiltonian into a power series of $x = 1/\varepsilon t_g$. This way, one can collect the same orders of the expansion in the left-hand side and right-hand side of Eq. (8) and relate the elements of H_{DRAG} to the corrective fields (involved in $\tilde{H}_{\text{CPT}}$) and to elements of $S(t)$ order by order. We also need to expand the control fields of the DRAG frame Hamiltonian with respect to the adiabatic parameter x:

$$H_{\text{DRAG}}^{(n)}(t) = H_{\text{extra}}^{(n)}(t) + \bar{H}^{(n)}(t) + i[S^{(n+1)}(t), \Pi_u], \quad (B1)$$

where $n \geq 0$ corresponds to the order of the transformed Hamiltonian, and H_{extra} is a nontrivial expression generated by the lower orders of the transformation, and,

$$\bar{H}_{\text{CPT},\omega d}(t) = \frac{1}{x}\Pi_u + \sum_{n=0}^{\infty} x^n \bar{H}^{(n)}(t). \quad (B2)$$

Notice that this expansion essentially means that the constraints in Eqs. (10) and (11), and consequently the control fields $h_i(t)$ and $h_z(t)$ should be made perturbative with respect to the order of this expansion as well. Furthermore, the general form of the Hermitian operator $S(t)$ for a d-dimensional system can be written as

$$S(t) = \sum_i s_{i,z}(t)\Pi_i + \sum_{i=o,c}\sum_{m<n} s_{i,m,n}(t)\sigma_{m,n}^i. \quad (B3)$$

The zeroth- and first-order expressions of H_{extra} are as follows [38]:

$$H_{\text{extra}}^{(0)} = 0,$$

$$H_{\text{extra}}^{(1)} = i[S^{(1)}(t), H^{(0)}(t)] - \frac{1}{2}[S^{(1)}(t), [S^{(1)}(t), \Pi_u]]$$

$$- \dot{S}^{(1)}(t). \quad (B4)$$

Using Eqs. (B1) and (B4), we can solve for the constrains in Eqs. (10) and (11) to obtain the appropriate control elements in terms of different orders of the parameter x. The control constraints of Eq. (10) turn into

$$\sqrt{2}\bar{\Omega}_o^{(n)} = h_o^{(n)} - \text{Tr}[H_{\text{extra}}^{(n)}(t)\sigma_{B,t}^o],$$

$$\sqrt{2}\bar{\Omega}_c^{(n)} = h_c^{(n)} - \text{Tr}[H_{\text{extra}}^{(n)}(t)\sigma_{B,t}^c], \quad (B5)$$

$$\bar{\delta}^{(n)}(t) = h_z^{(n)}(t) - \text{Tr}[H_{\text{extra}}^{(n)}(t)(\Pi_B - \Pi_t)].$$

Note that we pick the two original drives to have the same pulse envelope $\Omega_{0,o}(t) = \Omega_{1,o(t)} \equiv \Omega_o(t)$, and we set $\Omega_{0,c}(t) = \Omega_{1,c}(t) \equiv \Omega_c(t)$. This will implement an X rotation. A Y rotation can be implemented in a similar manner, except that the two original drives will have a $\pi/2$ phase difference. The phase difference, however, will not show up in the CPT frame and thus, the rest of the analysis will be identical in both cases. The decoupling constraints of Eq. (11) turn into

$$s_{c,D,u}^{(n+1)} = -\frac{1}{2}\text{Tr}[H_{\text{extra}}^{(n)}(t)\sigma_{D,u}^o] - \frac{1}{2\sqrt{2}}(\lambda_0 - \lambda_1)\bar{\Omega}_o^{(n)},$$

$$s_{o,D,u}^{(n+1)} = +\frac{1}{2}\text{Tr}[H_{\text{extra}}^{(n)}(t)\sigma_{D,u}^c] + \frac{1}{2\sqrt{2}}(\lambda_0 - \lambda_1)\bar{\Omega}_c^{(n)},$$

$$s_{c,B,u}^{(n+1)} = -\frac{1}{2}\text{Tr}[H_{\text{extra}}^{(n)}(t)\sigma_{B,u}^o] - \frac{1}{2\sqrt{2}}(\lambda_0 + \lambda_1)\bar{\Omega}_o^{(n)},$$

$$s_{o,B,u}^{(n+1)} = +\frac{1}{2}\text{Tr}[H_{\text{extra}}^{(n)}(t)\sigma_{B,u}^c] + \frac{1}{2\sqrt{2}}(\lambda_0 + \lambda_1)\bar{\Omega}_c^{(n)},$$

$$s_{c,t,u}^{(n+1)} = -\frac{1}{2}\text{Tr}[H_{\text{extra}}^{(n)}(t)\sigma_{t,u}^o],$$

$$s_{o,t,u}^{(n+1)} = +\frac{1}{2}\text{Tr}[H_{\text{extra}}^{(n)}(t)\sigma_{t,u}^c]. \quad (B6)$$

From these constraints, we first find the zeroth-order solutions. According to the CPT framework, in order to implement X rotations we set $h_o^{(0)}(t) = \sqrt{2}t_g\Omega(t)$ where $\Omega(t) = \sigma\,\text{sech}(\sigma t)$, $h_c^{(0)}(t) = 0$, and $h_z^{(0)}(t) = t_g\delta$. This implies that the target CPT Hamiltonian has the form:

$$H_{\text{target}}^{\text{CPT}} = [\sigma\,\text{sech}(\sigma t)\sigma_{B,t} + \text{h.c.}]. \quad (B7)$$

Note that the higher orders of $h_o^{(n)}$ and $h_c^{(n)}$ are set to zero, such that we obtain the desired evolution as dictated by the target Hamiltonian. Since we made our choice for the control fields $h(t)$, by making use of $H_{\text{extra}}^{(0)} = 0$ we can now solve for the pulse envelopes, from which we find

$$\Omega_o(t) = \sqrt{2}\Omega(t), \quad \Omega_c = 0. \quad (B8)$$

This ensures that we have the right form in the bright-target subspace of $H_{\text{DRAG}}^{(0)}$ to match the corresponding

bright-target elements of the target Hamiltonian. (Notice that the additional factor of $\sqrt{2}$ is present due to the CPT frame transformation.) Next, we proceed with the zeroth-order decoupling constraints. These constraints together with the zeroth-order target constraints will fix certain elements of $S^{(1)}(t)$, such that we essentially satisfy $H_{\mathrm{DRAG}}^{(0)} \equiv H_{\mathrm{target}}^{\mathrm{CPT}}$. Given the fact that $H_{\mathrm{extra}}^{(0)} = 0$, we find based on Eqs. (B6) that the nonzero elements of $S^{(1)}(t)$ are $s_{c,D,u}^{(1)} = -\frac{1}{2\sqrt{2}}(\lambda_0 - \lambda_1)t_g\Omega(t)$, and $s_{c,B,u}^{(1)} = -\frac{1}{2\sqrt{2}}(\lambda_0 + \lambda_1)t_g\Omega(t)$. These two constraints ensure no transitions between dark-unwanted and bright-unwanted states, respectively. The first-order corrective controls are found by satisfying the first-order target constraints. In this first order, as we already mention we set all the first-order control fields to zero. Making use of Eqs. (B5), we find the following equations:

$$\sqrt{2}\bar{\Omega}_o^{(1)} = 2\dot{s}_{o,B,t}^{(1)} + 2\delta s_{c,B,t}^{(1)},$$

$$\sqrt{2}\bar{\Omega}_c^{(1)} = 2\left(\dot{s}_{c,B,t}^{(1)} + \sqrt{2}\Omega t_g(s_{z,D}^{(1)} - s_{z,B}^{(1)}) - 2\delta s_{o,B,t}^{(1)}\right),$$

$$s_{c,B,t}^{(1)} = \frac{1}{16\sqrt{2}}[(\lambda_0 + \lambda_1)^2\,\Omega t_g$$
$$+ 8(\dot{s}_{z,D}^{(1)} - \dot{s}_{z,B}^{(1)})(\Omega t_g)^{-1}].$$
$$\text{(B9)}$$

To seek the simplest solution, which satisfies the $S^{(1)}(0) = S^{(1)}(t_g) = 0$ (such that the implemented gate is the same in the DRAG and CPT frame), we pick the free parameters $s_{z,i}^{(1)}$'s and $s_{o,B,t}^{(1)}$ all equal to zero. Substituting $s_{c,B,t}^{(1)}$ into the first two equations, we find the pulse corrections given in Eqs. (12) and (13) (notice that we require an additional factor of $\sqrt{2}$ in the non-CPT frame to accommodate for the CPT transformation). Substituting these solutions and the choices we made above for the generative elements of $S^{(1)}(t)$ in the expansion Eq. (B1) will lead to the first-order form of the DRAG Hamiltonian $H_{\mathrm{DRAG}}^{(1)}(t)$ given in Eq. (15). Note that since we terminate the expansion in the first order we set $S^{(2)}(t) = 0$.

---

[1] M. V. Gurudev Dutt, Jun Cheng, Bo Li, Xiaodong Xu, Xiaoqin Li, P. R. Berman, D. G. Steel, A. S. Bracker, D. Gammon, Sophia E. Economou, Ren-Bao Liu, and L. J. Sham, Stimulated and Spontaneous Optical Generation of Electron Spin Coherence in Charged GaAs Quantum Dots, Phys. Rev. Lett. **94**, 227403 (2005).

[2] Sophia E. Economou, L. J. Sham, Yanwen Wu, and D. G. Steel, Proposal for optical U(1) rotations of electron spin trapped in a quantum dot, Phys. Rev. B **74**, 205415 (2006).

[3] Sophia E. Economou and T. L. Reinecke, Theory of Fast Optical Spin Rotation in a Quantum Dot Based on Geometric Phases and Trapped States, Phys. Rev. Lett. **99**, 217401 (2007).

[4] Andrea Donarini, Michael Niklas, Michael Schafberger, Nicola Paradiso, Christoph Strunk, and Milena Grifoni, Coherent population trapping by dark state formation in a carbon nanotube quantum dot, Nat. Commun. **10**, 381 (2019).

[5] Samuel G. Carter, Stefan C. Badescu, Allan S. Bracker, Michael K. Yakes, Kha X. Tran, Joel Q. Grim, and Daniel Gammon, Coherent Population Trapping Combined with Cycling Transitions for Quantum Dot Hole Spins using Triplet Trion States, Phys. Rev. Lett. **126**, 107401 (2021).

[6] Arian Vezvaee, Girish Sharma, Sophia E. Economou, and Edwin Barnes, Driven dynamics of a quantum dot electron spin coupled to a bath of higher-spin nuclei, Phys. Rev. B **103**, 235301 (2021).

[7] E. M. Kessler, S. Yelin, M. D. Lukin, J. I. Cirac, and G. Giedke, Optical Superradiance from Nuclear Spin Environment of Single-Photon Emitters, Phys. Rev. Lett. **104**, 143601 (2010).

[8] Brian B. Zhou, Alexandre Baksic, Hugo Ribeiro, Christopher G. Yale, F. Joseph Heremans, Paul C. Jerger, Adrian Auer, Guido Burkard, Aashish A. Clerk, and David D. Awschalom, Accelerated quantum control using superadiabatic dynamics in a solid-state lambda system, Nat. Phys. **13**, 330 (2016).

[9] Brian B. Zhou, Paul C. Jerger, V. O. Shkolnikov, F. Joseph Heremans, Guido Burkard, and David D. Awschalom, Holonomic Quantum Control by Coherent Optical Excitation in Diamond, Phys. Rev. Lett. **119**, 140503 (2017).

[10] Christopher G. Yale, F. Joseph Heremans, Brian B. Zhou, Adrian Auer, Guido Burkard, and David D. Awschalom, Optical manipulation of the berry phase in a solid-state spin qubit, Nat. Photonics **10**, 184 (2016).

[11] W. C. Campbell, J. Mizrahi, Q. Quraishi, C. Senko, D. Hayes, D. Hucul, D. N. Matsukevich, P. Maunz, and C. Monroe, Ultrafast Gates for Single Atomic Qubits, Phys. Rev. Lett. **105**, 090502 (2010).

[12] K. Toyoda, K. Uchida, A. Noguchi, S. Haze, and S. Urabe, Realization of holonomic single-qubit operations, Phys. Rev. A **87**, 052307 (2013).

[13] Hiroki Takahashi, Ezra Kassa, Costas Christoforou, and Matthias Keller, Strong Coupling of a Single Ion to an Optical Cavity, Phys. Rev. Lett. **124**, 013602 (2020).

[14] L.-M. Duan, Geometric manipulation of trapped ions for quantum computation, Science **292**, 1695 (2001).

[15] J. Mizrahi, C. Senko, B. Neyenhuis, K. G. Johnson, W. C. Campbell, C. W. S. Conover, and C. Monroe, Ultrafast Spin-Motion Entanglement and Interferometry with a Single Atom, Phys. Rev. Lett. **110**, 203001 (2013).

[16] Katrina Barnes, *et al.*, Assembly and coherent control of a register of nuclear spin qubits, Nat. Commun. **13**, 2779 (2022).

[17] Adam Kinos, David Hunger, Roman Kolesov, Klaus Mølmer, Hugues de Riedmatten, Philippe Goldner, Alexandre Tallaire, Loic Morvan, Perrine Berger, Sacha Welinski, Khaled Karrai, Lars Rippe, Stefan Kröll, and Andreas Walther, Roadmap for rare-earth quantum computing (2021).

[18] Adam Kinos, Lars Rippe, Stefan Kröll, and Andreas Walther, Designing gate operations for single-ion quantum computing in rare-earth-ion-doped crystals, Phys. Rev. A **104**, 052624 (2021).

[19] S. L. Bayliss, D. W. Laorenza, P. J. Mintun, B. D. Kovos, D. E. Freedman, and D. D. Awschalom, Optically addressable molecular spins for quantum information processing, Science **370**, 1309 (2020).

[20] G. Falci, A. La Cognata, M. Berritta, A. D'Arrigo, E. Paladino, and B. Spagnolo, Design of a lambda system for population transfer in superconducting nanocircuits, Phys. Rev. B **87**, 214515 (2013).

[21] N. Earnest, S. Chakram, Y. Lu, N. Irons, R. K. Naik, N. Leung, L. Ocola, D. A. Czaplewski, B. Baker, Jay Lawrence, Jens Koch, and D. I. Schuster, Realization of a Λ System with Metastable States of a Capacitively Shunted Fluxonium, Phys. Rev. Lett. **120**, 150504 (2018).

[22] András Gyenis, Pranav S. Mundada, Agustin Di Paolo, Thomas M. Hazard, Xinyuan You, David I. Schuster, Jens Koch, Alexandre Blais, and Andrew A. Houck, Experimental Realization of a Protected Superconducting Circuit Derived from the 0–π Qubit, PRX Quantum **2**, 010339 (2021).

[23] V. O. Shkolnikov and Guido Burkard, Effective Hamiltonian theory of the geometric evolution of quantum systems, Phys. Rev. A **101**, 042101 (2020).

[24] Alexandre Baksic, Ron Belyansky, Hugo Ribeiro, and Aashish A. Clerk, Shortcuts to adiabaticity in the presence of a continuum: Applications to itinerant quantum state transfer, Phys. Rev. A **96**, 021801 (2017).

[25] Hugo Ribeiro, Alexandre Baksic, and Aashish A. Clerk, Systematic Magnus-Based Approach for Suppressing Leakage and Nonadiabatic Errors in Quantum Dynamics, Phys. Rev. X **7**, 011021 (2017).

[26] Zhi-Cheng Shi, Hai-Ning Wu, Li-Tuo Shen, Jie Song, Yan Xia, X. X. Yi, and Shi-Biao Zheng, Robust single-qubit gates by composite pulses in three-level systems, Phys. Rev. A **103**, 052612 (2021).

[27] W. Gao, A. Imamoglu, H. Bernien, and R. Hanson, Coherent manipulation, measurement and entanglement of individual solid-state spins using optical fields, Nat. Photonics **9**, 363 (2015).

[28] Ditte Møller, Lars Bojer Madsen, and Klaus Mølmer, Geometric phase gates based on stimulated Raman adiabatic passage in tripod systems, Phys. Rev. A **75**, 062302 (2007).

[29] J. H. Eberly and V. V. Kozlov, Wave Equation for Dark Coherence in Three-Level Media, Phys. Rev. Lett. **88**, 243604 (2002).

[30] M. Scala, B. Militello, A. Messina, and N. V. Vitanov, Stimulated Raman adiabatic passage in a Λ system in the presence of quantum noise, Phys. Rev. A **83**, 012101 (2011).

[31] Daniel Finkelstein-Shapiro, Simone Felicetti, Thorsten Hansen, Tõnu Pullerits, and Arne Keller, Classification of dark states in multilevel dissipative systems, Phys. Rev. A **99**, 053829 (2019).

[32] A. Kiely and A. Ruschhaupt, Inhibiting unwanted transitions in population transfer in two- and three-level quantum systems, J. Phys. B: At., Mol. Opt. Phys. **47**, 115501 (2014).

[33] L.-A. Wu and D. A. Lidar, Qubits as parafermions, J. Math. Phys. **43**, 4506 (2002).

[34] Sophia E. Economou, Juan I. Climente, Antonio Badolato, Allan S. Bracker, Daniel Gammon, and Matthew F. Doty, Scalable qubit architecture based on holes in quantum dot molecules, Phys. Rev. B **86**, 085319 (2012).

[35] Sergey Novikov, T. Sweeney, J. Robinson, Shavindra Premaratne, B. Suri, F. Wellstood, and B. Palmer, Raman coherence in a circuit quantum electrodynamics lambda system, Nat. Phys. **12**, 75 (2015).

[36] F. Motzoi, J. M. Gambetta, P. Rebentrost, and F. K. Wilhelm, Simple Pulses for Elimination of Leakage in Weakly Nonlinear Qubits, Phys. Rev. Lett. **103**, 110501 (2009).

[37] F. Motzoi and F. K. Wilhelm, Improving frequency selection of driven pulses using derivative-based transition suppression, Phys. Rev. A **88**, 062318 (2013).

[38] J. M. Gambetta, F. Motzoi, S. T. Merkel, and F. K. Wilhelm, Analytic control methods for high-fidelity unitary operations in a weakly nonlinear oscillator, Phys. Rev. A **83**, 012308 (2011).

[39] L. S. Theis, F. Motzoi, S. Machnes, and F. K. Wilhelm, Counteracting systems of diabaticities using drag controls: The status after 10 years (a), EPL **123**, 60001 (2018).

[40] M. Werninghaus, D. J. Egger, F. Roy, S. Machnes, F. K. Wilhelm, and S. Filipp, Leakage reduction in fast superconducting qubit gates via optimal control, npj Quantum Inf. **7**, 14 (2021).

[41] N. Rosen and C. Zener, Double Stern-Gerlach experiment and related collision phenomena, Phys. Rev. **40**, 502 (1932).

[42] Note that the presented analysis will be exactly the same if we swap the definition of the unwanted and target levels and change the sign of the detuning.

[43] Charles Santori, David Fattal, Jelena Vuckovic, Glenn S. Solomon, and Yoshihisa Yamamoto, Single-photon generation with InAs quantum dots, New J. Phys. **6**, 89 (2004).

[44] Jonas Becker, Johannes Görlitz, Carsten Arend, M. Markham, and Christoph Becher, Ultrafast, all-optical coherent control of single silicon vacancy colour centres in diamond, Nat. Commun. **7**, 13512 (2016).

[45] Matthew E. Trusheim, *et al.*, Transform-Limited Photons from a Coherent Tin-Vacancy Spin in Diamond, Phys. Rev. Lett. **124**, 023602 (2020).

[46] F. Jelezko and J. Wrachtrup, Single defect centres in diamond: A review, Phys. Status Solidi (a) **203**, 3207 (2006).

[47] Mark D. Bowdrey, Daniel K. L. Oi, Anthony J. Short, Konrad Banaszek, and Jonathan A. Jones, Fidelity of single qubit maps, Phys. Lett. A **294**, 258 (2002).

[48] J. R. Schrieffer and P. A. Wolff, Relation between the Anderson and Kondo Hamiltonians, Phys. Rev. **149**, 491 (1966).

[49] Evangelia Takou and Sophia E. Economou, Optical control protocols for high-fidelity spin rotations of single SiV$^-$ and SnV$^-$ centers in diamond, Phys. Rev. B **104**, 115302 (2021).

[50] Arian Vezvaee, Paul Hilaire, Matthew F. Doty, and Sophia E. Economou, Deterministic Generation of Entangled Photonic Cluster States from Quantum Dot Molecules, Phys. Rev. Appl. **18**, L061003 (2022).

[51] David C. McKay, Christopher J. Wood, Sarah Sheldon, Jerry M. Chow, and Jay M. Gambetta, Efficient z gates for quantum computing, Phys. Rev. A **96**, 022330 (2017).